Proc. Natl. Acad. Sci. USA
Vol. 96, pp. 6183–6188, May 1999
Biophysics

Identification of the proton pathway in bacterial reaction centers: Inhibition of proton transfer by binding of Zn^{2+} or Cd^{2+}

(bacterial photosynthesis/*Rhodobacter sphaeroides*/metal binding/proton-coupled electron transfer)

M. L. PADDOCK, M. S. GRAIGE, G. FEHER, AND M. Y. OKAMURA*

Department of Physics, University of California-San Diego, 9500 Gilman Drive, La Jolla, CA 92093

Contributed by G. Feher, March 22, 1999

ABSTRACT **The reaction center (RC) from *Rhodobacter sphaeroides* converts light into chemical energy through the light induced two-electron, two-proton reduction of a bound quinone molecule Q_B (the secondary quinone acceptor). A unique pathway for proton transfer to the Q_B site had so far not been determined. To study the molecular basis for proton transfer, we investigated the effects of exogenous metal ion binding on the kinetics of the proton-assisted electron transfer $k_{AB}^{(2)}$ ($Q_A^{-\bullet}Q_B^{-\bullet} + H^+ \rightarrow Q_A(Q_BH)^-$, where Q_A is the primary quinone acceptor). Zn^{2+} and Cd^{2+} bound stoichiometrically to the RC ($K_D \leq 0.5\ \mu M$) and reduced the observed value of $k_{AB}^{(2)}$ 10-fold and 20-fold (pH 8.0), respectively. The bound metal changed the mechanism of the $k_{AB}^{(2)}$ reaction. In native RCs, $k_{AB}^{(2)}$ was previously shown to be rate-limited by electron transfer based on the dependence of $k_{AB}^{(2)}$ on the driving force for electron transfer. Upon addition of Zn^{2+} or Cd^{2+}, $k_{AB}^{(2)}$ became approximately independent of the electron driving force, implying that the rate of proton transfer was reduced ($\geq 10^2$-fold) and has become the rate-limiting step. The lack of an effect of the metal binding on the charge recombination reaction $D^{+\bullet}Q_AQ_B^{-\bullet} \rightarrow DQ_AQ_B$ suggests that the binding site is located far (>10 Å) from Q_B. This hypothesis is confirmed by preliminary x-ray structure analysis. The large change in the rate of proton transfer caused by the stoichiometric binding of the metal ion shows that there is one dominant site of proton entry into the RC from which proton transfer to $Q_B^{-\bullet}$ occurs.**

The bacterial reaction center (RC) is a membrane-bound pigment protein complex that converts light into chemical energy through a two-electron, two-proton reduction of a bound quinone molecule Q_B (the secondary quinone acceptor) to a quinol molecule Q_BH_2 (1, 2). The protons taken up to form quinol are transferred from the solvent of the cytoplasm to the bound quinone molecule. Understanding the details of proton transfer in this and other systems is important for a basic understanding of bioenergetics. This paper addresses the pathway of the proton transfer by measuring the effects of metal ion binding on proton transfer rates in the bacterial RCs from *Rhodobacter sphaeroides*.

The isolated RC is composed of three polypeptide subunits (L, M, and H), four bacteriochlorophylls, two bacteriopheophytins, one internally bound nonheme Fe^{2+}, and two ubiquinone (UQ_{10}) molecules (reviewed in refs. 1 and 2). In the RC, the light-induced electron transfer proceeds from a primary donor (a bacteriochlorophyll dimer) through a series of electron donor and acceptor molecules (a bacteriopheophytin and a primary quinone acceptor Q_A) to a loosely bound secondary quinone Q_B, which serves as a mobile electron and proton carrier (3–5), transferring electrons and protons from the RC to other components of the bioenergetic cycle.

The first electron transfer to Q_B ($k_{AB}^{(1)}$) does not involve direct protonation of the quinone (Eq. **1**).

$$Q_A^{-\bullet}Q_B \rightarrow Q_AQ_B^{-\bullet}. \qquad [1]$$

However, the second electron transfer ($k_{AB}^{(2)}$) is coupled to the direct protonation of the quinone (Eq. **2a**). Subsequent protonation (Eq. **2b**) leads to the formation of quinol.

$$Q_A^{-\bullet}Q_B^{-\bullet} + H^+ \overset{\text{fast}}{\rightleftharpoons} Q_A^{-\bullet}Q_BH^{\bullet} \overset{\text{slow}}{\longrightarrow} Q_AQ_BH^- \qquad [2a]$$

$$Q_AQ_BH^- + H^+ \rightarrow Q_AQ_BH_2. \qquad [2b]$$

In native RCs from *Rb. sphaeroides*, the proton-coupled electron transfer reaction $k_{AB}^{(2)}$ (Eq. **2a**) was shown to be a two-step process in which fast protonation precedes rate-limiting electron transfer (6). The value of $k_{AB}^{(2)}$ in native RCs is, therefore, not a direct measure of the rate of proton transfer. However, when the proton transfer rate is sufficiently reduced, proton transfer becomes the rate-limiting step as has been observed in the site-directed mutation of Asp-L213 to Asn (7). To determine which of the two steps in Eq. **2a** is rate limiting, a driving-force assay, based on the free-energy dependence of $k_{AB}^{(2)}$, has been used (6).

The pathways for proton transfer have been studied by a number of groups (8–13). Results of $k_{AB}^{(2)}$ measurements on site-directed mutants had shown the importance of several amino acid residues, e.g., Glu-L212, Ser-L223, and Asp-L213, for the proton transfer reactions (Eq. **2**) (reviewed in refs. 14 and 15). These residues can be connected to the external surface through a number of possible proton transfer pathways and an internal carboxylic acid cluster that have been resolved in the crystal structures of the RC (16–19). Which of these is functionally the most important pathway had not been determined.

A complementary approach to site-directed mutagenesis, to identify residues involved in proton transfer, is to assess the effect of metal binding on the kinetics of proton transfer (Eq. **2**). In solution, metal ions bind to acidic and uncharged amine or imidazole groups (20). In a protein, these groups are provided by carboxylic acids and histidine residues. For example, the binding of Cu^{2+} has an inhibitory effect on proton transfer in carbonic anhydrase (21–23).

Utschig *et al.* (24) have shown that Zn^{2+} binds to the RC and affects the rate of transfer of the first electron $k_{AB}^{(1)}$ (Eq. **1**). We have confirmed their findings and have extended the work

The publication costs of this article were defrayed in part by page charge payment. This article must therefore be hereby marked "*advertisement*" in accordance with 18 U.S.C. §1734 solely to indicate this fact.

PNAS is available online at www.pnas.org.

Abbreviations: D, primary donor; Q_A, primary quinone acceptor; Q_B, secondary quinone acceptor; Q, quinone molecule; Q_{10}, coenzyme Q_{10} (2,3-dimethoxy-5-methyl-6-decaisoprenyl-1,4-benzoquinone); RC, reaction center; NQ, naphthoquinone; UQ, ubiquinone.

*To whom reprint requests should be addressed. e-mail: mokamura@ucsd.edu.

to an investigation of the effect of Zn^{2+} and Cd^{2+} binding on the proton-coupled electron transfer $k_{AB}^{(2)}$ (Eq. **2a**). In addition, we have investigated the driving-force dependence of $k_{AB}^{(2)}$, to establish which of the two steps in Eq. **2a** is rate limiting. Furthermore, we have measured the effects of the metal ions on the charge recombination rate constant k_{BD} ($D^{+\bullet}Q_AQ_B^{-\bullet} \rightarrow DQ_AQ_B$, where D is the primary donor), which is sensitive to the electrostatic potential near Q_B. By localizing the position of the bound cation, the location of the site of proton entry into the RC from which proton transfer to $Q_B^{-\bullet}$ occurs.

METHODS

Reagents and Quinones. The quinones Q_{10} (coenzyme Q_{10}; 2,3-dimethoxy-5-methyl-6-decaisoprenyl-1,4-benzoquinone) and MQ_4 (menatetrenone; 2-methyl-3-tetraisoprenyl-1,4-naphthoquinone) were obtained from Sigma. ADMNQ (2,6-dimethyl-3-undecyl-1,4,-naphthoquinone) and ATMNQ (2,6,7-trimethyl-3-undecyl-1,4,-naphthoquinone) were kindly provided by Andreas Labahn (Albert-Ludwigs Universität, Freiburg, Germany) (25). All quinones were prepared in ethanol before their use. The Q_B site inhibitors terbutryne and stigmatellin were obtained from Chem Service (West Chester, PA) and Fluka, respectively, and were prepared in ethanol. Cytochrome *c* from horse heart was obtained from Sigma and was reduced (>95%) by hydrogen gas on platinum black (Aldrich) and filtered (0.2-μM pore size acetate filter). All other reagents were of analytical grade.

Isolation and Preparation of RCs. RCs from *Rb. sphaeroides* R26 were isolated in 15 mM Tris·HCl, pH 8, 0.025% lauryl dimethylamine-*N*-oxide (LDAO), 1 mM EDTA following published procedures (26) as modified by Utschig *et al.* (27). Both Q_A and Q_B were removed as described (28, 29) to yield RCs with $\leq$ 10% residual Q_A/RC and $\leq$ 0.2% residual Q_B/RC, as measured at 865 nm from the charge recombination rate and amplitude (28). The ratio of absorbance, A^{280}/A^{800}, was 1.20. Substitution of a naphthoquinone (NQ) for the native UQ at the Q_A site was performed as described (6, 30).

Reconstitution of the Q_B site was achieved by incubation of the solubilized RC solution with Q_{10} adsorbed to celite (diatomaceous earth, Fisher) for ≈20 min at 25°C while stirring (6) or by addition of Q_{10} (≈3 Q_{10} per RC) solubilized in 1% LDAO. Occupancy of the Q_B sites varied from 50% to 80% over the range of pH studied.

Transient Optical Spectroscopy. Charge recombination rates were measured by monitoring the recovery of the donor band at 865 nm after bleaching with a single laser flash (Phase R DL2100c, 590 nm, ≈0.2 J/pulse, 0.4-μs full-width-half-max) by using a single-beam spectrophotometer (31). All measurements were performed at 21°C. To determine the $D^+Q_AQ_B^{-\bullet} \rightarrow DQ_AQ_B$ recombination rate (k_{BD}), the observed absorption decays were fitted to multiple exponentials by using procedures previously described (30). To measure the $D^+Q_A^{-\bullet} \rightarrow DQ_A$ recombination rate (k_{AD}), electron transfer from $Q_A^{-\bullet}$ to Q_B was blocked by the addition of 100 μM terbutryn or 10 μM stigamatellin. For studies of the driving-force dependence of rates, NQs were substituted into the Q_A site. The relative occupancies of the NQ and UQ in the Q_A site were determined from a deconvolution of the charge recombination kinetics (6), because k_{AD} is different for NQ and UQ (6, 30).

The rate constant ($k_{AB}^{(1)}$) for the transfer of the first electron to Q_B (Eq. **1**) was measured by monitoring the bacteriopheophytin bandshift at 750 nm, which is sensitive to the reduction state of the quinones Q_A and Q_B (31, 32). To improve the signal-to-noise ratios, 9–36 traces were averaged.

The proton-coupled electron transfer $k_{AB}^{(2)}$ (Eq. **2a**) was determined by monitoring the decay of the semiquinone absorption at 450 nm after a second saturating laser flash in the presence of an external reductant (10 μM horse heart cytochrome *c*) (33). In RCs with a NQ added to occupy the Q_A site (see above), biphasic kinetics were observed with one rate corresponding to the rate observed in RCs with UQ_{10} occupying the Q_A site ($k_{AB}^{(2)} \approx 1{,}200\ s^{-1}$, pH 7.5, native RCs without a heavy metal) and the other rate corresponding to RCs with a NQ occupying the Q_A site ($k_{AB}^{(2)} \approx 6{,}000\ s^{-1}$, pH 7.5, native RCs without a heavy metal). The relative occupancies of UQ_{10} and NQ determined in this manner agreed with the relative occupancies determined from the deconvolution of biphasic kinetics for k_{AD}.

EPR Spectroscopy. The light-induced EPR spectra of RC samples in the presence and in the absence of 10 mM $ZnSO_4$ and $CdSO_4$ were obtained on a spectrometer of local design at a microwave frequency of 9 GHz (34). The samples were concentrated to $A_{800}^{1cm} \approx 77$, frozen in a 15×6×1-mm flat quartz cell and illuminated in the frozen state by a 500-W projector lamp (34).

RESULTS

Binding of Exogenous Metal Ions to the RC. The measured value of $k_{AB}^{(2)}$ (Eq. **2a**) was used as functional assay for heavy metal binding to the RC. Most of the heavy metals compounds that were tested ($MnSO_4$, $CuSO_4$, $ZnSO_4$, $CdSO_4$, $HgCl_2$) caused a decrease in the observed rate at 1 mM concentrations, except for $FeSO_4$, which had no effect at this concentration. However, only the addition of $CdSO_4$ and $ZnSO_4$ caused a significant decrease in the observed rate at 10 μM concentrations (Fig. 1). These two metals became, therefore, the focus of our investigation. The disparate results obtained with different compounds show that the observed effect on $k_{AB}^{(2)}$ is not caused by the anionic counterion (i.e., SO_4^{2-}), which was the same for all of the metals tested, except $HgCl_2$.

Measurements of Charge Recombination. The charge recombination rates for the reactions $D^+Q_A^{-\bullet} \rightarrow DQ_A$ (k_{AD}) and $D^+Q_AQ_B^{-\bullet} \rightarrow DQ_AQ_B$ (k_{BD}) were measured at 865 nm in the presence and absence of an exogenous cation. The measured values of k_{AD} (≈9 s^{-1}) and k_{BD} (≈ 0.8 s^{-1}) were the same with or without exogenous Zn^{2+} or Cd^{2+} (Table 1). The amplitude of the k_{BD} phase remained unchanged upon addition of Zn^{2+} or Cd^{2+}. Similarly the pH profile of k_{BD} was essentially the same with or without Zn^{2+} or Cd^{2+} (data not shown).

Measurements of the First Electron Transfer Rate $k_{AB}^{(1)}$. The measured rates of transfer for the first electron to Q_B ($k_{AB}^{(1)}$, Eq. **1**), measured at 750 nm, were reduced ≈10-fold upon addition of 10 μM Zn^{2+} or Cd^{2+} (Table 1). The slower observed rate constant was independent of the metal concentration above 10 μM. At cation concentrations below 10 μM, we could deconvolute the observed kinetics into two phases, one phase at 7,000 s^{-1} (the rate observed without exogenous cations) and one phase at 700 s^{-1} (the rate observed at ≥10 μM concentration). From the dependence of the amplitude of the slow phase with cation concentration, we estimated a dissociation constant (K_D) of ≤0.5 μM for Zn^{2+} and Cd^{2+} (data not shown).

Measurements of the Proton-Coupled Electron Transfer Rate $k_{AB}^{(2)}$. The rate of transfer for the second electron to Q_B ($k_{AB}^{(2)}$, Eq. **2a**), after the second saturating laser flash at 450 nm, was measured in native RCs to be 1,200 s^{-1} at pH 8 (Table 1). Upon addition of 10 μM Zn^{2+} or Cd^{2+}, $k_{AB}^{(2)}$ decreased to a limiting value of 120 s^{-1} and 60 s^{-1}, respectively (Table 1). The effect of the metal on the rate was observed immediately after addition without an incubation period. The fraction of the sample exhibiting the slower rate depended on the concentration of the cations (Fig. 2) and allowed us to estimate a dissociation constant (K_D) of ≤0.5 μM for Zn^{2+} and Cd^{2+}, which is, within experimental error, the same as that determined from the $k_{AB}^{(1)}$ measurements.

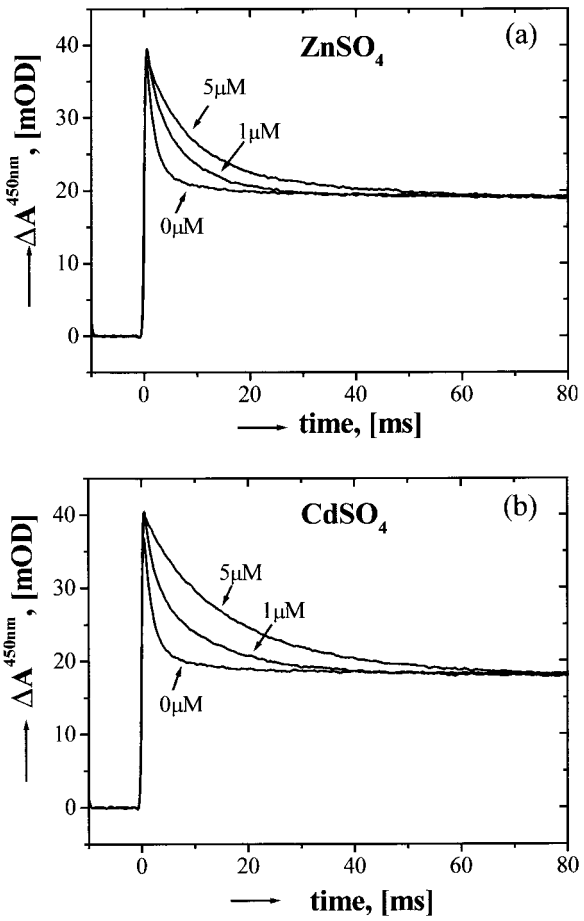

FIG. 1. Absorbance decay of the semiquinones at 450 nm as a function of time after the second of two laser flashes in the presence of various concentrations of $ZnSO_4$ (*a*) and $CdSO_4$ (*b*). From the decay, the rate constant $k_{AB}^{(2)}$ was determined. Note the slowing of the kinetics with increasing cation concentrations. The pedestal at long times after the laser flash is caused by the absorbance change of the cytochrome *c* used to reduce the primary donor (see *Materials and Methods*). Conditions were: 2 μM RCs in 10 mM Tris·HCl (pH 7.7), 0.25% lauryl dimethylamine-*N*-oxide with the concentration of $ZnSO_4$ or $CdSO_4$ as indicated in the figure.

The decrease in the value of $k_{AB}^{(2)}$ caused by the addition of exogenous Zn^{2+} or Cd^{2+} was eliminated upon addition of EDTA (a strong chelater of cationic metals) to a concentration of twice the exogenous metal concentration. Further addition of Zn^{2+} or Cd^{2+} to twice that of the EDTA concentration led again to a reduced value of $k_{AB}^{(2)}$ to 120 s^{-1} or 60 s^{-1}, respectively.

Table 1. Measured rate constants for RCs in the presence and absence of metal ions (pH 8.0, T = 21°)

RCs*	k_{AD} (s^{-1})	k_{BD} (s^{-1})	$k_{AB}^{(1)}$ (s^{-1})†	$k_{AB}^{(2)}$ (s^{-1})
Native	8.8	0.8	7,000	1,200
Native + Zn^{2+}	8.8	0.7	700	120
Native + Cd^{2+}	9.0	0.8	700	60

Errors in the rates are estimated to be ~8% for the charge recombination rate constants k_{AD} and k_{BD} and ~15% for the forward electron transfer rate constants $k_{AB}^{(1)}$ and $k_{AB}^{(2)}$

*Conditions for kinetic measurements as described in *Materials and Methods*. The samples labeled Native + Zn^{2+} and Native + Cd^{2+} were measured in the presence of 10μM $ZnSO_4$ and $CdSO_4$, respectively.

†This is the observed rate constant using a single exponential fit to the data. This reaction can be better fitted with a sum of two exponentials (24), but the effect of the metal binding is clearly shown by using this simple analysis.

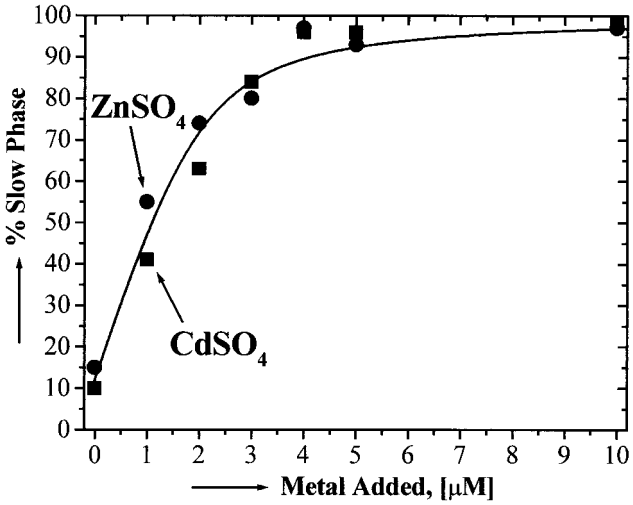

FIG. 2. Fraction of slow phase (A_{slow})of $k_{AB}^{(2)}$ as a function of the concentration of added $ZnSO_4$ (●) or $CdSO_4$ (■). The kinetics of Fig. 2 were decomposed into two components: $\Delta A^{450nm}(t) = A_{fast} \exp(-k_{fast}t) + A_{slow} \exp(-k_{slow}t)$, where k_{fast} = 1,200 s^{-1} (the observed rate without the addition of the metal) and k_{slow} = 120 s^{-1} or 60 s^{-1} (the observed rate upon addition of high concentrations of $ZnSO_4$ or $CdSO_4$, respectively). The solid curve is a fit to a standard binding equation with K_D = 0.3 μM. Conditions were the same as in Fig. 1.

The reduced value of $k_{AB}^{(2)}$ to 60 s^{-1} upon addition of 10 μM Cd^{2+} could be increased to 120 s^{-1} upon addition of 50 μM Zn^{2+}, showing that Zn^{2+} had replaced Cd^{2+}.

The pH profile of $k_{AB}^{(2)}$ was measured in a mixture of 2 mM Hepes, 2 mM Ches, 2 mM Mes in 0.025% lauryl dimethylamine-*N*-oxide buffer from pH 7 to 9.5 and in 0.04% maltoside from pH 5 to 9. The same values of $k_{AB}^{(2)}$ were observed in either detergent at the same pH. In the presence of Zn^{2+} or Cd^{2+}, the value of $k_{AB}^{(2)}$ decreased with increasing pH with a slope proportional to $[H^+]^{0.5}$ over the measured pH ranges (data not shown). This pH dependence differs from the native behavior where $k_{AB}^{(2)}$ decreases with pH proportional to $[H^+]^{0.3}$ below pH 5 and $[H^+]^{0.9}$ above pH 8.5.

Dependence of the Proton-Coupled Electron Transfer Rates on the Driving Force for Electron Transfer. The driving force for electron transfer was changed by replacing the native Q_{10} in the Q_A site with a series of NQs that have different redox potentials while retaining the native Q_{10} in the Q_B site. The experimental results on native RCs without a bound Zn^{2+} or Cd^{2+} showed an increase in the observed rate upon increasing the driving force for electron transfer. In the presence of Zn^{2+} and Cd^{2+}, $k_{AB}^{(2)}$ became approximately independent of the driving force for electron transfer (Fig. 3). The dependence of $k_{AB}^{(2)}$ on the driving force was restored to either sample by addition of EDTA to twice the concentration of that of the exogenous metal. Upon further addition of Zn^{2+} and Cd^{2+} to twice the EDTA concentration, $k_{AB}^{(2)}$ became again approximately independent of the driving force.

EPR Spectroscopy. The light-induced EPR specta of RCs frozen in the dark were measured in the presence and absence of Zn^{2+} and Cd^{2+}. All spectra were characteristic of the broad (≈300 G) Fe^{2+}-$Q^{-\bullet}$ complex at g = 1.8 with a ratio of Fe^{2+}-$Q^{-\bullet}/D^{+\bullet}$ of 1.0 ± 0.1 (34) (data not shown).

DISCUSSION

We investigated the effects of Zn^{2+} and Cd^{2+} binding to RCs on the transfer rate of the first electron, $k_{AB}^{(1)}$ (Eq. **1**), and on the rate of the proton-assisted second electron transfer, $k_{AB}^{(2)}$

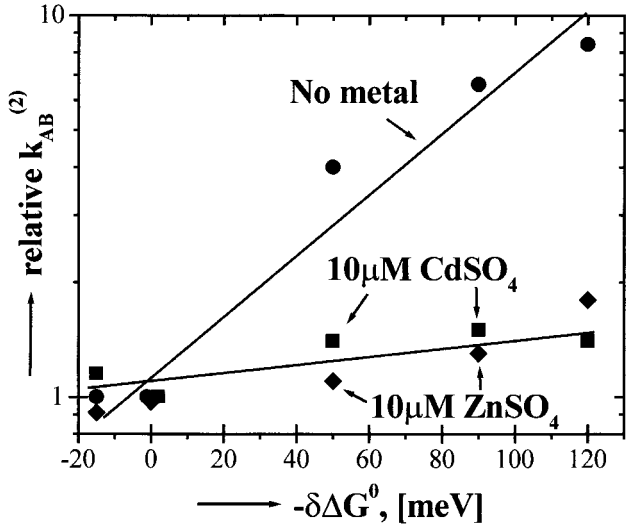

FIG. 3. The rate constant of proton-coupled second electron transfer, $k_{AB}^{(2)}$, in RCs as a function of the change in redox free energy (driving force) for electron transfer in the absence and in the presence of 10 μM Zn^{2+} and Cd^{2+}. Note that $k_{AB}^{(2)}$ in the absence of added metals show a "Marcus"-like dependence on the electron driving force characteristic of a rate-limited electron transfer reaction as has been reported (6), whereas in the presence of Zn^{2+} or Cd^{2+}, $k_{AB}^{(2)}$ is approximately independent of the electron driving force, showing that proton transfer (Eq. **3**) has become rate limiting. Quinones substituted into the Q_A site were from left to right: MQ_0, menadione (2-methyl-1,4-naphthoquinone); Q_{10}, coenzyme Q_{10}; MQ_4, menatetrenone (2-methyl-3-tetraisoprenyl-1,4-naphthoquinone); ADMNQ, 2,6-dimethyl-3-undecyl-1,4,-naphthoquinone; and ATMNQ, 2,6,7-trimethyl-3-undecyl-1,4,-naphthoquinone. Conditions were the same as in Fig. 1.

(Eq. **2a**). By localizing the binding site of Zn^{2+} and Cd^{2+} we identified the point of entry of the protons and the start of the proton transfer pathway(s) to $Q_B^{-\bullet}$.

The Effect of Zn^{2+} and Cd^{2+} Binding on $k_{AB}^{(1)}$. The rate of the first electron reduction $k_{AB}^{(1)}$ (Eq. **1**) was reduced $\approx$10-fold upon the binding of Zn^{2+} or Cd^{2+}. These findings confirm the results of Utschig *et al.* (24) on the effect of Zn^{2+} binding and show that a similar effect is found upon binding of Cd^{2+}.

The reaction mechanism of $k_{AB}^{(1)}$ in isolated RCs involves a slow rate-limiting gating step that involves the movement of Q_B (18) before electron transfer (35). Thus, the decreased rate upon binding Zn^{2+} or Cd^{2+} implies a slowing down of the conformational gating step. The movement of Q_B into the active position requires a rotation of the quinone head group and a displacement of several water molecules (17–19). The possibility that bound Zn^{2+} or Cd^{2+} directly hindered the quinone rotation and movement is excluded because a decrease in k_{BD} would be expected as discussed in a later section. A possible explanation advanced by Utschig *et al.* (24) is that cation binding alters protein conformation, thereby affecting protein dynamics that are necessary for $Q_B^{-\bullet}$ formation. One possibility is that bound Zn^{2+} or Cd^{2+} hinders the movement of water out of the RC through a contiguous water chain that was observed in the crystal structures of *Rb. sphaeroides* (16, 18, 19), thereby indirectly hindering the movement of Q_B into its active position. Another possible explanation is that Q_B reduction is slowed as a consequence of a slowing of the rate of proton uptake and/or redistribution of the protons that stabilize the semiquinone (36–40).

The Effect of Zn^{2+} and Cd^{2+} Binding on $k_{AB}^{(2)}$. The rate of the proton-coupled electron transfer $k_{AB}^{(2)}$ (Eq. **2a**) was reduced $\approx$10-fold and $\approx$20-fold upon addition of Zn^{2+} or Cd^{2+}, respectively. The mechanism of the $k_{AB}^{(2)}$ reaction was deduced from the dependence of the observed rate on the driving force for electron transfer (6). For RCs in the absence of cations, $k_{AB}^{(2)}$ depends on the electron transfer driving force (Fig. 3) consistent with a rate-limiting electron transfer after a fast proton transfer ($k_H+ \gg k_{AB}^{(2)}$, i.e., $\geq 10^4\ s^{-1}$) as was previously reported (6). In the presence of Zn^{2+} or Cd^{2+}, $k_{AB}^{(2)}$ is approximately independent of the driving force (Fig. 3), implying a change in the mechanism of the proton-coupled electron transfer. This conclusion is further supported by the change in the pH dependence of $k_{AB}^{(2)}$. The rate of proton transfer (first step of Eq. **2a**) now has become the rate-limiting step for the reaction (i.e., $k_{AB}^{(2)} = k_H+ \approx 10^2\ s^{-1}$), i.e.,

$$(Q_A^{-\bullet}Q_B^{-\bullet}) \text{ --- } M^{2+} + H^+ \xrightarrow{\text{slow}} (Q_A^{-\bullet}Q_BH^{\bullet}) \text{ --- } M^{2+}$$

$$(Q_A^{-\bullet}Q_BH^{\bullet}) \text{ --- } M^{2+} \xrightarrow{\text{fast}} (Q_AQ_BH^{-}) \text{ --- } M^{2+}, \quad [3]$$

where M^{2+} is either Zn^{2+} or Cd^{2+}. Thus, the rate of proton transfer to $Q_B^{-\bullet}$ is reduced from $k_H+ \geq 10^4\ s^{-1}$ without a bound metal ion to $k_H+ \approx 10^2\ s^{-1}$ with a bound metal ion (i.e., a $\geq$$10^2$-fold reduction). The reduced rate of proton transfer upon stoichiometric binding of Zn^{2+} or Cd^{2+} implies that there is one dominant site of proton entry into the RC that is blocked by the bound metal ion.

In RCs with a bound Zn^{2+} or Cd^{2+}, $k_{AB}^{(2)}$ is a measure of the rate of proton transfer, which enables one to trace the proton transfer pathway from $Q_B^{-\bullet}$ to the surface of the RC by measuring $k_{AB}^{(2)}$ in a series of site-directed mutant RCs. These studies should provide insight into the rates of proton conduction in the RC.

Characterization and Localization of the Binding Site of Zn^{2+} and Cd^{2+}: Identification of the Dominant Proton Transfer Pathway. The competitive replacement of Cd^{2+} by Zn^{2+} shows that both metal ions bind to the same or to nearby positions on the RC. The stoichiometry of the kinetic effects was found to be $\approx$1 metal cation per RC. The dissociation constants for Zn^{2+} and Cd^{2+} were determined to be $K_D \leq 0.5$ μM.

We now turn to a discussion of the location of the Zn^{2+} and Cd^{2+} binding site(s). The light-induced, low-temperature EPR spectrum, which is characteristic of the Fe^{2+}-$Q^{-\bullet}$ complex, excludes the possibility that either Zn^{2+} or Cd^{2+} displaces the Fe^{2+} in the interior of the RC. The measured recombination kinetics, k_{BD}, in the presence of Zn^{2+} and Cd^{2+} show that there are no electrostatic or structural changes near Q_B. Thus, a direct interaction between $Q_B^{-\bullet}$ and the bound Zn^{2+} or Cd^{2+} is excluded.

The most likely location(s) of the metal ions would be a surface accessible region that is rich in His, Glu, and/or Asp residues. There are three surface accessible His residues (H68, H126, H128) forming a cluster located $\approx$20 Å from the Q_B binding site at the surface of the H subunit (Fig. 4); this cluster previously was proposed as a possible Zn^{2+} binding location by Utschig *et al.* (24). His-H68 is located near one of the termini of the possible proton transfer pathway P1 (Fig. 4). His-H126 and His-H128 are located closer to P3 (Fig. 4).

There are also several surface accessible carboxylic acid residues (Asp-L210, Asp-M17, Asp-H124, Glu-H224, Asp-M240). Three of these carboxylic acid groups are components of a larger cluster of carboxylic acid residues located $\approx$10 Å from Q_B and near P3 (Fig. 4), which was proposed to act as a local proton reservoir (13).

The most direct way of determining the binding location of Zn^{2+} and Cd^{2+} is by x-ray diffraction. Preliminary x-ray diffraction results have been obtained by H. L. Axelrod, E. C. Abresch, M.L.P., M.Y.O., and G.F. (unpublished work), which show that Cd^{2+} and Zn^{2+} are ligated to His-H126, His-H128, and Asp-H124 (see Fig. 4). Thus, this region of the RC surface

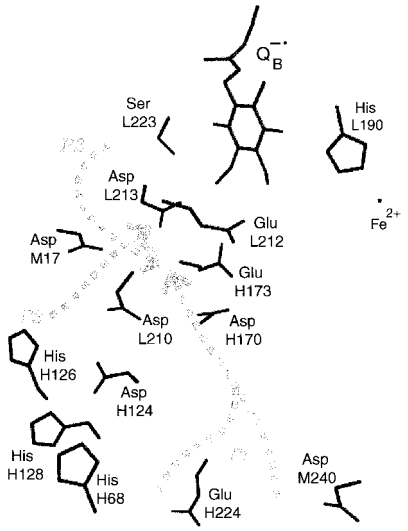

FIG. 4. Part of the RC structure near the secondary quinone, Q_B binding site, as determined for the Q_B^- state by Stowell *et al.* (18). Possible proton transfer pathways (P1–P3) proposed by Abresch *et al.* (19) are shown by dashed lines. One carbonyl oxygen of Q_B is located near Ser-L223 and the backbone NH of Ile-L224 (not shown); the other carbonyl oxygen of Q_B is located near His-L190. Nearby are two carboxylic acid groups Asp-L213 and Glu-L212 that have been implicated in proton transfer to reduced Q_B (reactions **2a** and **2b**, respectively) (8–13) and to which the proton transfer pathways lead. Also shown are a His cluster (consisting of H68, H126, and H128) and a carboxylic acid cluster (consisting of Asp-L213, Asp-L210, Asp-M17, Glu-H173, Asp-H170, and Asp-M124).

has been identified as being crucial for fast physiological proton transfer from solution to the bound $Q_B^{-\bullet}$.

The Mechanism of Proton Conduction in the Bacterial RC. The binding of Cd^{2+} or Zn^{2+} to the surface accessible region on the H-subunit (His-H126, His-H128, and Asp-H124) results in a drastic reduction ($\geq 10^2$-fold) in the rate of proton transfer. The simplest explanation for the inhibition of proton transfer is that one or more of these three residues function as proton donors. The binding of Cd^{2+} in the vicinity of P3 reduces their effectiveness as a source of protons.

An alternate explanation is that the binding of the metal ion creates a barrier for proton entry into one of the proton transfer pathways that have been proposed (8–15, 19, 41–43). In this view, the bound cation may electrostatically hinder proton uptake. The pathway most likely to be involved is P3 (19) (Fig. 4). Yet another explanation is that the metal ion binding affects the protein dynamics as has been postulated to be the cause for the changed kinetic for $k_{AB}^{(1)}$ (24).

SUMMARY

The results of the binding of Zn^{2+} and Cd^{2+} to RCs from *Rb. sphaeroides* can be summarized as follows:

(*i*) Zn^{2+} and Cd^{2+} bind nearly stoichiometrically at or near the same position on the RC with a dissociation constant $K_D \leq 0.5$ μM.

(*ii*) The first electron transfer rate, $k_{AB}^{(1)}$ (Eq. **1**), is reduced $\approx$10-fold, implying a slowing down of the conformational gating step.

(*iii*) The proton transfer rate to $Q_B^{-\bullet}$ is reduced $\gg 10^2$-fold, making it the rate-limiting step in the $k_{AB}^{(2)}$ reaction (Eq. **2a**).

(*iv*) The large reduction ($\gg 10^2$-fold) in the rate of proton transfer upon stoichiometric binding implies that there is one dominant proton entry point into the RC.

(*v*) Preliminary x-ray studies localized the Cd^{2+} and Zn^{2+} binding site near His-H126, His-H128, and Asp-H124.

(*vi*) The simplest explanation of the inhibitory effects of Zn^{2+} and Cd^{2+} on the proton transfer rate is that their binding to the histidine and aspartic acid residues reduces their effectiveness as proton donors.

Note Added in Proof. The proposal that the slow rate of proton transfer (Eq. **3**) is caused by disruption of the proton donor(s) or blockage of the proton transfer pathway is supported by recent results from the effect of mutations on the observed rate. Replacement of either Asp-M17 or Asp-L210 with Asn resulted in an additional ~10-fold reduction in the observed rate (at 1 mM Cd^{2+}) from that observed in native RCs. Because the mutation sites are located close to P3 (Fig. 4), these results show that proton transfer in the presence of Cd^{2+} proceeds through P3 or a pathway near P3.

In addition to Zn^{2+} and Cd^{2+}, we found that Co^{2+} and Ni^{2+} reduced $k_{AB}^{(2)}$ by ~40-fold and ~100-fold, respectively.

We thank Herb Axelrod and Ed Abresch for permission to quote their unpublished results, Roger Isaacson and Ed Abresch for technical assistance, and Andreas Labahn for the ADMNQ (2,6-dimethyl-3-undecyl-1,4,-naphthoquinone) and ATMNQ (2,6,7-trimethyl-3-undecyl-1,4,-naphthoquinone). This work was supported by the National Science Foundation (NSF MCB94–16652) and National Institutes of Health (GM 41637 and GM 13191).

1. Breton, J. & Vermeglio, A., eds. (1988) *The Photosynthetic Bacterial Reaction Center, Structure, and Dynamics* (Plenum, New York).
2. Feher, G., Allen, J. P., Okamura, M. Y. & Rees, D. C. (1989) *Nature (London)* **339,** 111–116.
3. Crofts, A. R. & Wraight, C. A. (1983) *Biochim. Biophys. Acta* **726,** 149–185.
4. Maroti, P. & Wraight, C. A. (1990) in *Current Research in Photosynthesis*, ed. Baltscheffsky, M. (Kluwer, Boston), Vol. 1, pp. 1.165–1.168.
5. Gunner, M. (1991) *Curr. Topics Bioenerg.* **16,** 319–367.
6. Graige, M. S., Paddock, M. L., Bruce, J. M., Feher, G. & Okamura, M. Y. (1996a) *J. Am. Chem. Soc.* **118,** 9005–9016.
7. Paddock, M. L., Senft, M. E., Graige, M. S., Ronsey, S. H., Toranchik, T., Feher, G. & Okamura, M. Y. (1998) *Photosynth. Res.* **55,** 281–291.
8. Paddock, M. L., Rongey, S. H., Feher, G. & Okamura, M. Y. (1989) *Proc. Natl. Acad. Sci. USA* **86,** 6602–6606.
9. Takahashi, E. & Wraight, C. A. (1990) *Biochim. Biophys. Acta* **1020,** 107–111.
10. Takahashi, E. & Wraight, C. A. (1992) *Biochemistry* **31,** 855–866.
11. Paddock, M. L., Rongey, S. H., McPherson, P. H., Juth, A., Feher, G. & Okamura, M. Y. (1994) *Biochemistry* **33,** 734–745.
12. Baciou, L. & Michel, H. (1995) *Biochemistry* **34,** 7967–7972.
13. Takahashi, E. & Wraight, C. A. (1996) *Proc. Natl. Acad. Sci. USA* **93,** 2640–2645.
14. Takahashi, E. & Wraight, C. A. (1994) in *Advances in Molecular and Cell Biology*, ed. Barbar, J. (JAI Press, Greenwich, CT), pp. 197–251.
15. Okamura, M. Y. & Feher, G. (1995) in *Anoxygenic Photosynthetic Bacteria*, eds. Blankenship, R. E., Madigan, M. T. & Bauer, C. E. (Kluwer, Dordrecht, The Netherlands), pp. 577–594.
16. Ermler, U., Fritzsch, G., Buchanan, S. K. & Michel, H. (1994) *Structure (London)* **2,** 925–936.
17. Lancaster, C. R. D., Michel, H., Honig, B. & Gunner, M. R. (1996) *Biophys. J.* **70,** 2469–2492.
18. Stowell, M. H. B., McPhillips, T. M., Rees, D. C., Soltis, S. M., Abresch, E. & Feher, G. (1997) *Science* **276,** 812–816.
19. Abresch, E. C., Paddock, M. L., Stowell, M. H. B., McPhillips, T. M., Axelrod, H. L., Soltis, S. M., Rees, D. C., Okamura, M. Y. & Feher, G. (1998) *Photosynth. Res.* **55,** 119–125.
20. Lewis, J. & Wilkins, L., eds. (1960) *Modern Coordination Chemistry* (Interscience, New York).
21. Eriksson, A. E., Jones, T. A. & Liljas, A. (1986) in *Zinc Enzymes,* eds. Bertini, I., Luchinat, C., Maret, W. & Zeppezauer, M. (Birkhauser, Boston), pp. 317–328.
22. Tu, C., Wynns, G. C. & Silverman, D. N. (1981) *J. Biol. Chem.* **256,** 9466–9470.
23. Hurt, J. D., Tu, C., Laipis, P. J. & Silverman, D. N. (1997) *J. Biol. Chem.* **272,** 13512–13518.
24. Utschig, L. M., Ohigashi, Y., Thurnauer, M. C. & Tiede, D. M. (1998) *Biochemistry* **37,** 8278–8281.

25. Schmid, R., Goebel, F., Warnecke, A. & Labahn, A. (1999) *J. Chem. Soc., Perkin Trans.*, in press.
26. Isaacson, R. A., Lendzian, F., Abresch, E. C., Lubitz, W. & Feher, G. (1995) *Biophys. J.* **69,** 311–322.
27. Utschig, L. M., Greenfield, S. R., Tang, J., Laible, P. D. & Thurnauer, M. C. (1997) *Biochemistry* **36,** 8548–8558.
28. Okamura, M. Y., Isaacson, R. A. & Feher, G. (1975) *Proc. Natl. Acad. Sci. USA* **72,** 3491–3495.
29. Woodbury, N. W., Parson, W. W., Gunner, M. R., Prince, R. C. & Dutton, P. L. (1986) *Biochim. Biophys. Acta* **851,** 6–22.
30. Labahn, A., Bruce, J. M., Okamura, M. Y. & Feher, G. (1995) *Chem. Phys.* **197,** 355–366.
31. Kleinfeld, D., Okamura, M. Y. & Feher, G. (1984) *Biochim. Biophys. Acta* **766,** 126–140.
32. Vermeglio, A. & Clayton, R. K. (1977) *Biochim. Biophys. Acta* **461,** 159–165.
33. Kleinfeld, D., Okamura, M. Y. & Feher, G. (1985) *Biochim. Biophys. Acta* **809,** 291–310.
34. Butler, W. F., Calvo, R., Fredkin, D. R., Isaacson, R. A., Okamura, M. Y. & Feher, G. (1984) *Biophys. J.* **45,** 947–973.
35. Graige, M. S., Feher, G. & Okamura, M. Y. (1998) *Proc. Natl. Acad. Sci. USA* **95,** 11679–11684.
36. Miksovska, J., Kálmán, L., Schiffer, M., Maróti, P., Sebban, P. & Hanson, D. K. (1997) *Biochemistry* **36,** 12216–12226.
37. McPherson, P. H., Okamura, M. Y. & Feher, G. (1988) *Biochim. Biophys. Acta* **934,** 348–368.
38. Maroti, P. & Wraight, C. A. (1988) *Biochim. Biophys. Acta* **934,** 314–328.
39. Nabedryk, E., Breton, J., Hienerwadel, R., Fogel, C., Mäntele, W., Paddock, M. L. & Okamura, M. Y. (1995) *Biochemistry* **34,** 14722–14732.
40. Maroti, P. & Wraight, C. A. (1997) *Biophys. J.* **73,** 367–381.
41. Sebban, P., Maróti, P. & Hanson, D. K. (1995) *Biochimie* **77,** 677–694.
42. Beroza, P., Fredkin, D. R., Okamura, M. Y. & Feher, G. (1992) in *The Photosynthetic Bacterial Reaction Center II*, eds. Breton, J. & Vermeglio, A. (Plenum, New York), pp. 363–374.
43. Allen, J. P., Feher, G., Yeates, T. O., Komiya, H. & Rees, D. C. (1987) *Proc. Natl. Acad. Sci USA* **84,** 6162–6166.